Supplementary information for radiative consequences of low-temperature infrared refractive indices for supercooled water clouds

Penny M. Rowe*[1], Steven Neshyba[2] & Von P. Walden[1]

[1]Department of Geography, University of Idaho, Moscow, ID, 83844 USA

[2]Department of Chemistry, University of Puget Sound, Tacoma, WA, 98416 USA .

[3]Department of Department of Civil and Environmental Engineering, Washington State University, Pullman, WA, 99164, USA

Correspondence to: P. M. Rowe (prowe@harbornet.com)

Supplementary Methods: Atmospheric models. Five sets of atmospheric profiles were created: tropical, mid-latitude summer, mid-latitude winter, Arctic summer, and Arctic winter. The Arctic summer and Arctic winter profiles use radiosoundings made by Environment Canada at Eureka, Canada, obtained from the Integrated Global Radiosonde Archive (IGRA; Durre et al., 2006). For atmospheric pressure, temperature, and relative humidity, the mean values recorded by the radiosondes for summers and winters between 2006 and 2008 are used. The relative humidity is converted to partial pressure (ppmv), set to 5 ppmv above 10 km, and scaled so that the total precipitable water vapor agrees with measurements made by a microwave radiometer (Liljegren et al., 1996). The ozone profile was determined from the mean of several ozonesondes, scaled to agree with total ozone measurements (CRESTech, & MSC. World Ozone and Ultraviolet Radiation Data Centre (WOUDC) [Data]. Retrieved January 5, 2010, from http://www.woudc.org). The CO_2 amount was set to 390 ppmv. Other trace gas concentrations are

based on surface measurements made at Barrow, Alaska (CH_4: Duglokencky et al., 2012; CO: Novelli et al., 2012 and N_2O, F11, F12, and F113 from the NOAA/ESRL halocarbons in situ program), or on the subarctic winter standard model (McClatchey et al. 1972). The midlatitude summer and winter and the tropical model atmospheres use standard atmosphere models (McClatchey et al. 1972). Model atmospheric profiles extend from 0 to 60 km (although the maximum height used in simulations was between 25 and 60 km). Profiles are comprised of between 33 and 45 layers; more layers are needed for warmer, wetter atmospheres. For each simulation, the humidity was modified so that the RH was 100% at the cloud height. Profiles of temperature and humidity are shown in Supplementary Fig. 1. Approximate positions of model clouds are indicated by circles.

Supplementary Methods: Single scattering parameters. Indices of refraction were used to create single-scattering parameters as a function of effective radius and wavenumber. Single-scattering properties were calculated using Mie theory in the manner described by Neshyba et al. (2003; see also references within), summarized as follows. The extinction efficiency, single-scattering albedo, and phase function were computed for cloud droplets with radii spanning 0.1-230 μm, at intervals of 0.0333 in $\log_{10}$ space. The single-scattering properties were then computed in a log-normal distribution about a geometric mean radius, r_g,

$$r_g = r_e / \exp\left(2.5 \ln(\sigma_g)\right),$$

where r_e specifies and effective radius and $\sigma_g = 0.331$ was chosen for these calculations. The distribution was truncated at $\pm 4\sigma_g$, which typically resulted in ~35 individual radii contributing to any given distribution. Gaussian quadrature was used to infer Legendre expansion coefficients

from phase functions in such a way that the forward peak of the phase function matched the value of the phase function at 0.25° away from forward scattering (McFarlane et al., 2004).

Supplementary Methods: Radiance and Flux simulations. Radiance and flux simulations make use of clear and cloudy-sky atmospheric optical depths. Clear-sky optical depths are calculated using each of the five model atmospheric profiles as input to the Line-By-Line-Radiative-Transfer Program (LBLRTM version 11.6; Clough et al., 2005), using the HITRAN database for lineshape parameters (Rothman et al., 2005). Clouds are set in the model atmosphere layers in which temperatures are close to 263K, 253K, and 240K (except for the Arctic winter, for which the warmest tropospheric temperature is 249K). Cloud optical depth is calculated and combined with the corresponding (same atmospheric layer) clear-sky optical depth, for a variety of liquid water paths (LWP; 0.1 to 100 g m^{-2}) and particle effective radii (5, 10, and 15 μm). These, together with the single-scattering parameters derived from the complex refractive indices (CRI), and other necessary parameters described below, are then inputted into a program for Discrete-Ordinate-method Radiative Transfer in scattering and emitting layered media (DISORT; Stamnes et al., 1988).

DISORT was used to calculate cloudy-sky surface and top-of-atmosphere spectral fluxes for the entire hemisphere [in units of W m^{-2} (cm^{-1})] both at the TOA and at the surface. To maximize accuracy, both LBLRTM and DISORT are run in double precision, and at least 16 streams are used in DISORT. Spectral fluxes are calculated for the new, temperature-dependent CRI and for the 300K CRI (Downing and Williams, 1975; reference given in manuscript).

In preparation for running DISORT, single-scattering parameters corresponding to the desired

CRI are interpolated to each effective radius and wavenumber. The cloud LWP is converted to a wavenumber-dependent cloud optical depth. The cloud layer is selected based on the cloud height, and the cloud optical depth is combined with the clear-sky optical depth in this layer. Ice clouds are not included, and the sun is assumed to be below the horizon for all the simulations. The surface is assumed to be Lambertian. For the Arctic and midlatitude winter, an ice/snow surface is assumed, while for the tropical model an ocean surface is used (MODIS emissivity library: http://www.icess.ucsb.edu/modis/EMIS/html/em.html). For the midlatitude summer a surface emissivity model for the continental U.S. is used (45° latitude, 100° longitude; Seemann et al., 2007).

Supplementary Results

Upwelling and downwelling flux differences are shown in Supplementary Tables 1 and 2, for clouds at 263K, 253K, and 240K (except for the AW model, for which the highest tropospheric temperature was 249K). The magnitudes of the flux differences increase with decreasing temperature, as the temperature-dependent CRI becomes increasingly different from the 300K CRI. The magnitudes of the flux differences decrease with increasing r_e. The largest effect on upwelling radiances is for the tropics, where the 300K CRI overestimates the flux, relative to the temperature-dependent CRI, by 1 to 3 W m^{-2} for r_e of 5 to 10 μm and cloud temperatures of 240 to 253K. The largest effect on downwelling radiances is for similar clouds in the Arctic winter, for which the 300K CRI underestimates the flux, relative to the temperature-dependent CRI, by 1 to 2 W m^{-2}.

Supplementary Table 1. Differences in cloudy-sky downwelling flux due to complex refractive indices (CRI) used for supercooled liquid clouds. Flux differences are calculated at the surface over the spectral region 460 to 990 cm^{-1} for fluxes calculated using CRI measured at 300K minus those for temperature-dependent CRI, for a variety of atmospheric models: Arctic summer (AS), Arctic winter (AW), midlatitude summer (MS), midlatitude winter (MW) and tropical (TRP); cloud temperatures (T) and heights (H); liquid water paths (LWP; g/m^2); and cloud droplet effective radii (r_e, μm).

Atm. model	cloud T (K)	cloud H (km)	flux difference (W/m^2)								
			LWP=4			LWP=8			LWP=11		
			r_e=5	r_e=10	r_e=15	r_e=5	r_e=10	r_e=15	r_e=5	r_e=10	r_e=15
AW	240	0.1	-1.50	-0.79	-0.38	-1.25	-0.88	-0.49	-0.93	-0.81	-0.50
AW	249	1.1	-1.67	-0.86	-0.39	-1.35	-0.95	-0.51	-0.99	-0.86	-0.51
AW	240	3.8	-1.61	-0.85	-0.41	-1.38	-0.95	-0.53	-1.06	-0.88	-0.55
MLW	263	2.5	-1.27	-0.47	-0.15	-1.09	-0.53	-0.21	-0.84	-0.50	-0.21
MLW	253	4.4	-1.48	-0.57	-0.20	-1.28	-0.66	-0.27	-0.99	-0.62	-0.28
MLW	240	6.5	-1.60	-0.67	-0.27	-1.41	-0.77	-0.37	-1.12	-0.73	-0.38
AS	263	3.2	-1.09	-0.38	-0.12	-0.95	-0.44	-0.16	-0.75	-0.42	-0.16
AS	253	5.0	-1.32	-0.49	-0.17	-1.16	-0.57	-0.23	-0.92	-0.54	-0.24
AS	240	6.2	-1.42	-0.56	-0.22	-1.27	-0.66	-0.29	-1.10	-0.63	-0.31
MLS	263	5.7	-0.59	-0.19	-0.05	-0.56	-0.23	-0.06	-0.45	-0.22	-0.07
MLS	253	7.3	-0.73	-0.25	-0.07	-0.68	-0.30	-0.10	-0.55	-0.29	-0.11
MLS	240	9.3	-0.83	-0.31	-0.12	-0.79	-0.39	-0.17	-0.65	-0.37	-0.18
TRP	263	7.7	-0.36	-0.11	-0.02	-0.35	-0.13	-0.03	-0.29	-0.13	-0.04
TRP	253	6.1	-0.44	-0.14	-0.04	-0.43	-0.18	-0.05	-0.35	-0.17	-0.06
TRP	240	9.7	-0.51	-0.19	-0.07	-0.50	-0.24	-0.10	-0.42	-0.24	-0.11

Supplementary Table 2. Differences in cloudy-sky upwelling flux due to complex refractive indices (CRI) used for supercooled liquid clouds. Flux differences are calculated at the surface over the spectral region 460 to 990 cm^{-1} for fluxes calculated using CRI measured at 300K minus those for temperature-dependent CRI, for a variety of atmospheric models: Arctic summer (AS), Arctic winter (AW), midlatitude summer (MS), midlatitude winter (MW) and tropical (TRP); cloud temperatures (T) and heights (H); liquid water paths (LWP; g/m^2); and cloud droplet effective radii (r_e, μm).

Atm. model	cloud T (K)	cloud H (km)	flux difference (W/m^2)								
			LWP=4			LWP=8			LWP=11		
			r_e=5	r_e=10	r_e=15	r_e=5	r_e=10	r_e=15	r_e=5	r_e=10	r_e=15
AW	240	0.1	0.13	0.05	0.03	0.17	0.07	0.04	0.20	0.08	0.04
AW	249	1.1	-0.02	-0.03	-0.00	0.10	-0.01	0.00	0.20	0.02	0.01
AW	240	3.8	0.52	0.26	0.14	0.62	0.32	0.18	0.66	0.34	0.19
MLW	263	2.5	0.51	0.20	0.09	0.54	0.25	0.12	0.51	0.25	0.13
MLW	253	4.4	1.19	0.52	0.23	1.16	0.61	0.30	1.04	0.60	0.31
MLW	240	6.5	2.04	1.00	0.47	1.93	1.14	0.61	1.68	1.10	0.63
AS	263	3.2	0.66	0.26	0.11	0.67	0.31	0.14	0.61	0.31	0.15
AS	253	5.0	1.40	0.61	0.26	1.35	0.71	0.34	1.20	0.69	0.36
AS	240	6.2	1.99	0.93	0.18	1.88	1.07	0.24	1.63	1.04	0.58
MLS	263	5.7	1.18	0.46	0.18	1.13	0.54	0.24	1.00	0.53	0.25
MLS	253	7.3	2.08	0.90	0.38	1.92	1.02	0.49	1.65	0.99	0.51
MLS	240	9.3	3.15	1.50	0.70	2.88	1.71	0.90	2.41	1.63	0.93
TRP	263	7.7	1.31	0.53	0.20	1.25	0.60	0.26	1.10	0.59	0.28
TRP	253	6.1	2.24	0.99	0.40	2.07	1.10	0.52	1.76	1.06	0.54
TRP	240	9.7	3.36	1.65	0.74	3.06	1.81	0.95	2.56	1.73	0.98

Supplementary References

Clough S. A. et al.: Atmospheric radiative transfer modeling: a summary of the AER codes. *J. Quant. Spectrosc. Radiat. Transf.* 91(2):233-244, 2005.

Dlugokencky E. J., Lang P. M., Crotwell A. M., and Masarie K. A.: Atmospheric Methane Dry Air Mole Fractions from the NOAA ESRL Carbon Cycle Cooperative Global Air Sampling Network, 1983-2011, Version: 2012-09-24, Path: ftp://ftp.cmdl.noaa.gov/ccg/ch4/flask/event/, 2012.

Durre I., Vose R. S., Wuertz D. B.: Overview of the Integrated Global Radiosonde Archive. *J. Clim.* 19:53–68 doi:10.1175/JCLI3594.1, 2006.

Liljegren J. C., Lesht B. M.: Measurements of integrated water vapor and cloud liquid water from microwave radiometers at the DOE ARM cloud and radiation testbed in the U.S. Southern Great Plains, paper presented at International Geoscience and Remote Sensing Symposium, IEEE, Lincoln, Nebr., doi:10.1109/IGARSS.1996.516767, 1996.

McClatchey R. A., Fenn R. W., Selby J. E. A., Volz F. E., Garing J. S.: *Optical properties of the atmosphere, 3rd ed., Tech. Rep. AFCRL- 72–0497*, 108 pp., Air Force Geophys. Lab., Hanscom AFB, Mass., 1972.

McFarlane S. A., Evans K. F.: Clouds and shortwave fluxes at Nauru. Part II: Shortwave flux closure. *J. Atmos. Sci.* 61:2602-2615, 2004.

Neshyba S. P., Grenfell T. C., and Warren S. G.: Representation of a nonspherical ice particle by a collection of independent spheres for scattering and absorption of radiation: 2. Hexagonal columns and plates. *J. Geophys. Res.* 108:4448, doi:10.1029/2002JD003302, 2003.

Novelli P. C. and Masarie K. A.: Atmospheric Carbon Monoxide Dry Air Mole Fractions from the NOAA ESRL Carbon Cycle Cooperative Global Air Sampling Network, 1988-2011, Version: 2012-09-18, Path: ftp://ftp.cmdl.noaa.gov/ccg/co/flask/event, 2012.

Rothman L. S. et al.: The 2004 molecular spectroscopic database. *J. Quant. Spectrosc. Radiat. Transf.* 96(2):139-204, 2005.

Seemann S. W., Borbas E. E., Knuteson R. O., Stephenson G. R., Huang H.-L.: Development of a Global Infrared Land Surface Emissivity Database for Application to Clear Sky Sounding Retrievals from Multi-spectral Satellite Radiance Measurements. *J. of Appl. Meteor. and Climatol.*, 47:108-123, 2007.

Stamnes K., Tsay S.-C., Wiscomb W., and Jayaweera K.: Numerically stable algorithm for discrete-ordinate-method radiative transfer in multiple scattering and emitting layered media. *Applied Optics* 27(12):2502:2509, 1988.

Figures

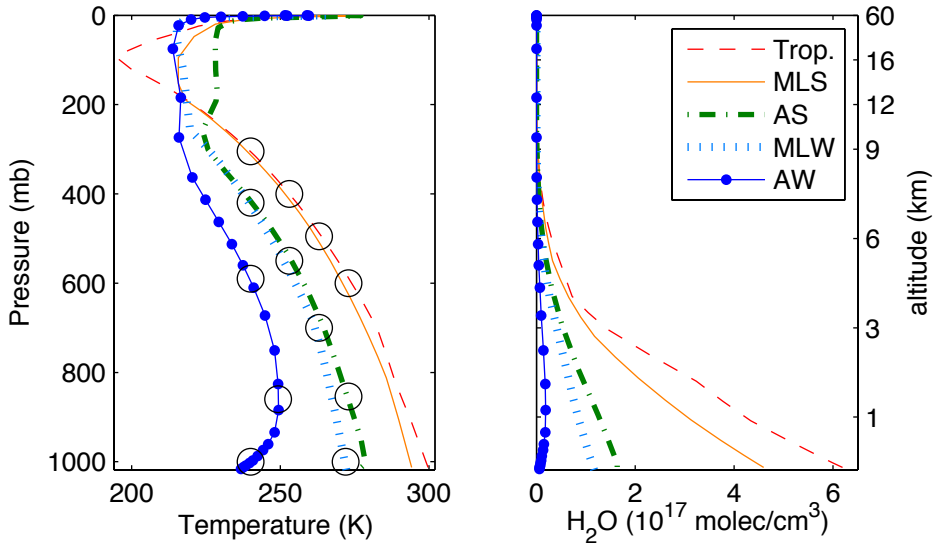

Supplementary Fig. 1. Atmospheric profiles of temperature (left panel) and water vapor (right panel) used for simulating fluxes for the tropical (Trop.), mid-latitude summer (MLS), Arctic summer (AS), mid-latitude winter (MLW), and Arctic winter (AW). Approximate positions of model clouds are indicated by black circles on the left hand panel (actual pressures/altitudes of clouds vary slightly with model).